Chapter 5 Dielectric Performance

A brief description of dielectric properties in Chapter 2 was presented about free/bound water transition determination by dielectric measurement techniques. This chapter expands on dielectric theory and its application to polymer relaxation, including a development of the electrical modulus representation of polarization processes. The dielectric properties of neat epoxy films and epoxy matrix/glass laminates are described both in terms of performance as interlayer dielectrics for PCB applications and as a tool in understanding some of the fundamental properties impacted by the presence of residual surfactant. Published work on dynamic dielectric and mechanical analysis of plasticized polymers and miscible polymer blends are reviewed, leading to a cooperativity analysis of the dielectric results of this study. This cooperativity analysis provides a more complete understanding of dielectric phenomena and related molecular relaxations in the PCB laminate materials.

5.1 Background and Literature Review

5.1.1 Dielectric Theory

When an electric field **E** is imposed upon a material, bound charges and charged particles within the material move to align with the field. The energy of the electric field incident upon the material is partially stored by the motion of charged species or by the realignment of polar groups within molecules. This storage phenomenon, which differentiates the material from free space, is a constitutive property of a specific material, and is described by the relative (real) permittivity, or dielectric constant ε'. The charge density arising from the aligned dipoles, known as the polarization field, **P**, only accounts for the bound part of the charge density in a material. The total electric charge flux density vector, **D,** is the sum of the free and bound charge displacements due to **E**:

Equation 5.1 $$\boldsymbol{D} = \varepsilon_0 \boldsymbol{E} + \boldsymbol{P}$$

where ε_0 is the permittivity of free space. The constitutive relation for a general material is

Equation 5.2 $$\boldsymbol{D} = \varepsilon_0 \varepsilon^* \boldsymbol{E}$$

so the polarization can be found by combining Equation 5.1 and Equation 5.2

Equation 5.3 $$\mathrm{P} = \varepsilon_0 (\varepsilon^* - 1)\mathrm{E}$$

where ε* is the complex permittivity.

There area several major polarization phenomena.[1] Dipoles fall into two categories: permanent and induced. Permanent dipoles have electrical asymmetry of charge groups in their molecular structure. Induced dipoles can result from either the shift in the electron cloud around the nucleus of an atom (electronic polarization) or from the relative displacement of nuclei because of unbalanced distribution of

charge in a molecule (atomic polarization). Inhomogeneous materials can experience Maxwell-Wagner polarization, which is the build-up of charges at the interfaces of dissimilar materials.

5.1.2 Complex Permittivity

As the electric field, **E,** oscillates at higher frequencies, polarized groups and dipoles tend to displace in-phase with **E**. These dipoles lose energy due to internal, anelastic, or frictional resistance and therefore begin to lag the phase of **E**. This behavior gives rise to the complex nature of the permittivity. The fundamental quantities that relate **E** and the current density **J** (a measure of displaced charge due to **E**) are conductivity σ and the complex relative permittivity ε^*. Note that the relative permittivity is a dimensionless complex coefficient of the free space permittivity ε_0; all subsequent references in this work to the permittivity ε^* imply that the quantity is relative. The current density can be written

$$\begin{aligned} \boldsymbol{J} &= j\omega\varepsilon_0\left(\varepsilon' - j\left[\varepsilon''_d + \frac{\sigma}{\omega\varepsilon_0}\right]\right)\boldsymbol{E} \\ &= j\omega\varepsilon_0\left(\varepsilon' - j\varepsilon''_{eff}\right)\boldsymbol{E} \\ &= j\omega\varepsilon_0\varepsilon^*\boldsymbol{E} \end{aligned}$$

Equation 5.4

Where the complex permittivity is defined to be

$$\varepsilon^* = \varepsilon' - j\varepsilon''_{eff}$$

Equation 5.5

Again, this complex permittivity is a relative quantity, therefore ε' and ε''_{eff} are the dimensionless relative dielectric constant and loss factor, respectively. The real and imaginary components of the permittivity for a given dielectric are not independent, but are related in the frequency-domain by the Kramers-Kronig relations[2]:

$$\varepsilon' = 1 + \frac{2}{\pi}\int_0^\infty \frac{\omega'\varepsilon''(\omega')}{(\omega')^2 - \omega^2}\, d\omega'$$

Equation 5.6

$$\varepsilon'' = \frac{2\omega}{\pi}\int_0^\infty \frac{1 - \varepsilon'(\omega')}{(\omega')^2 - \omega^2}\, d\omega'$$

Equation 5.7

where ω' is a dummy variable of integration.

The effective dielectric loss factor ε''_{eff} (to be known simply as ε'' hereafter) accounts for both mobile charge conductivity, σ, and dielectric loss mechanisms ε''_d. Furthermore, if all of the loss mechanisms, including Maxwell-Wagner charging, induced polarization, and dipole rotation, are considered to contribute to dielectric loss in Equation 5.5, the form

$$\varepsilon'' = \varepsilon''_{dp} + \varepsilon''_e + \varepsilon''_a + \varepsilon''_{mw} - \frac{\sigma}{\omega\varepsilon_0}$$

Equation 5.8

is obtained, where the subscripts dp, e, a, and mw refer to dipolar, electronic, atomic, and Maxwell-Wagner effects, respectively. These effects are schematically illustrated in Figure 5.1. Equation 5.8 represents the

total effective loss of the major polarization and conduction mechanisms in dielectric materials. A commonly encountered quantity that provides insight into the "lossiness", or dissipative quality relative to the storage capability, of a material is the loss tangent tan δ. The definition of tan δ can be written

Equation 5.9 $$\tan\delta = \frac{\varepsilon''_{eff}}{\varepsilon'} = \frac{\varepsilon''_{d} + \frac{\sigma}{\omega\varepsilon'}}{\varepsilon'}$$

In the case of a dielectric material where σ = 0, tan δ is the ratio of the imaginary to the real part of the permittivity.

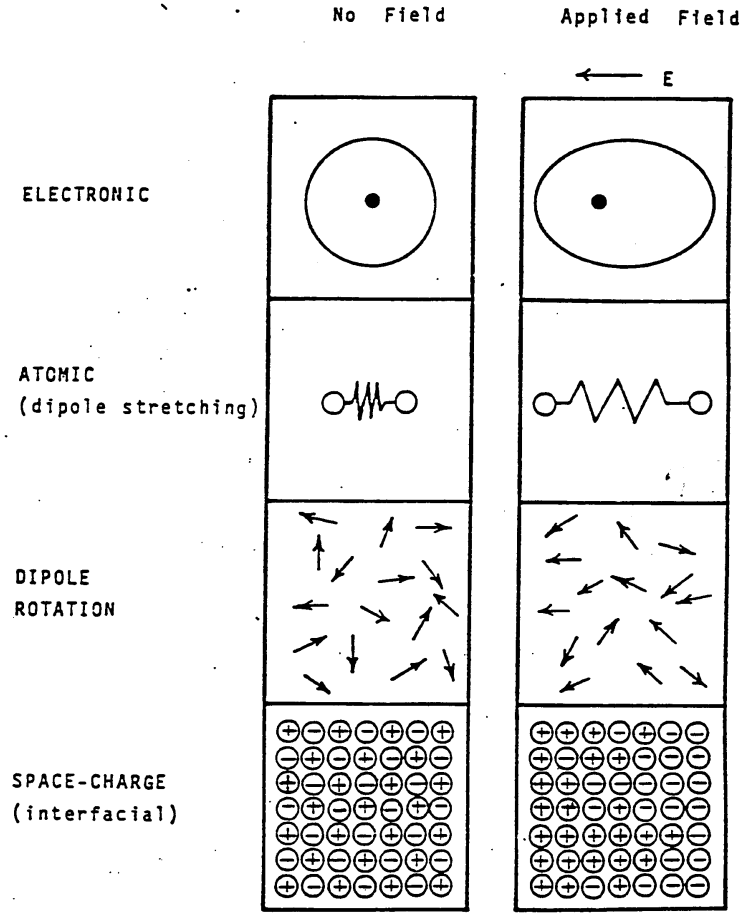

Figure 5.1: Electrical polarization modes[3]

The component materials used in this study, glass fibers and polymers, possess different responses, which are generally a function of frequency and temperature. It is important to note that since polymers are viscoelastic materials, many dielectric relaxation mechanisms are fundamentally related by time-temperature superposition principles. As temperatures increase, relaxation mechanisms that were more pronounced at lower frequencies shift toward higher frequencies; this is directly related to the increased mobility of molecular structures in bulk materials at higher temperatures.

5.1.2.1 Electrical Loss Mechanisms in Glass

At low frequencies, ion jump phenomena and DC conductivity effects dominate the dielectric properties in glass, while at microwave and radio frequencies the primary dielectric loss mechanisms are ion vibrations and deformation, and dipole relaxation.[4] Ion jump mechanisms are best illustrated by the example of a substitution ion and related vacancy forming a dipole pair in a crystal lattice, as shown in Figure 5.2. This pair will behave like a molecular dipole and will reorient and relax under an applied electric field. Ion vibrations involve the drift of ionized dopant atoms or contaminants under an applied field. This is especially important in crystalline materials where dopant ions migrate to the grain boundaries where they can move more easily than ions restricted in atomic lattices.[4] A summary of loss mechanisms as a function of frequency is presented in Figure 5.3. It should be noted that, in general, tan δ for most glasses is very small at room temperature; those glass systems with ionic dopants or contaminants will display a higher loss.

Figure 5.2: Reorientation of a lattice vacancy pair in glass[4]

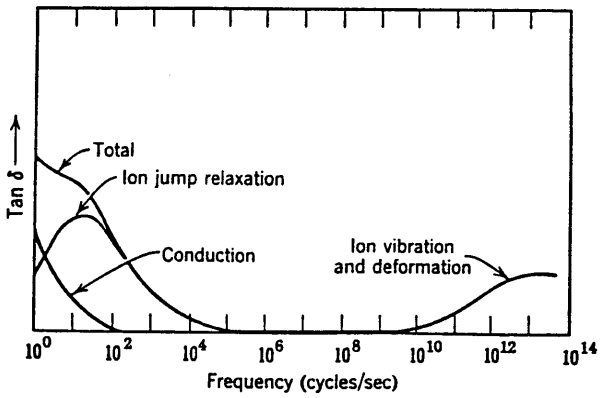

Figure 5.3: Room temperature dielectric loss mechanisms in glass at different frequencies[4]

5.1.2.2 Loss Mechanisms in Polymers

The complex nature of polymers, which include long molecular chains of varied backbone segment lengths, polar side groups, and semicrystalline phases, leads to several dielectric loss mechanisms. Each mechanism has an associated peak on a plot of tan δ with temperature or frequency. A schematic diagram of loss peaks for amorphous and semicrystalline polymers as a function of normalized temperature at 1 Hz is presented in Figure 5.4. One type of naming convention denotes the highest temperature loss peak as the

α peak, the next peak in descending temperature is the β peak, followed by γ, δ and so on.[5,6] In semicrystalline polymers the α peak occurs near the melt temperature T_m and is associated with the long-range motion of chains as they gain more freedom of motion in the melt. The β peak is associated with chain motion near the glass transition temperature T_g. Polar side group rotation, which can occur to some degree even in the glassy state, is responsible for the γ peak. The δ peak and any subsequent peaks, are the result of increasingly smaller polar group relaxation. In an amorphous polymer there is no α relaxation related to crystal melting, so the first peak is the β peak, associated with the main chain relaxation near the glass transition temperature.[7] The γ peak is associated with local segment or side group motion below T_g and subsequent peaks result from smaller polar group relaxation.

The epoxy system used in this study exhibited two relaxations, designated α and β, over the frequency-temperature ranges of the dielectric measurements. The higher temperature α relaxation is associated with the motion of polymer chain segments between cross-links. The sub-ambient temperature β relaxation, which involves the motion of structures on the sub-chain level, has been attributed to the rotation of –OH groups and crankshaft rotation of the glycidyl portion of the chain.[8] A γ relaxation has also been associated with the dielectric relaxations of unreacted epoxide groups; no γ relaxation was observed in this study.[8]

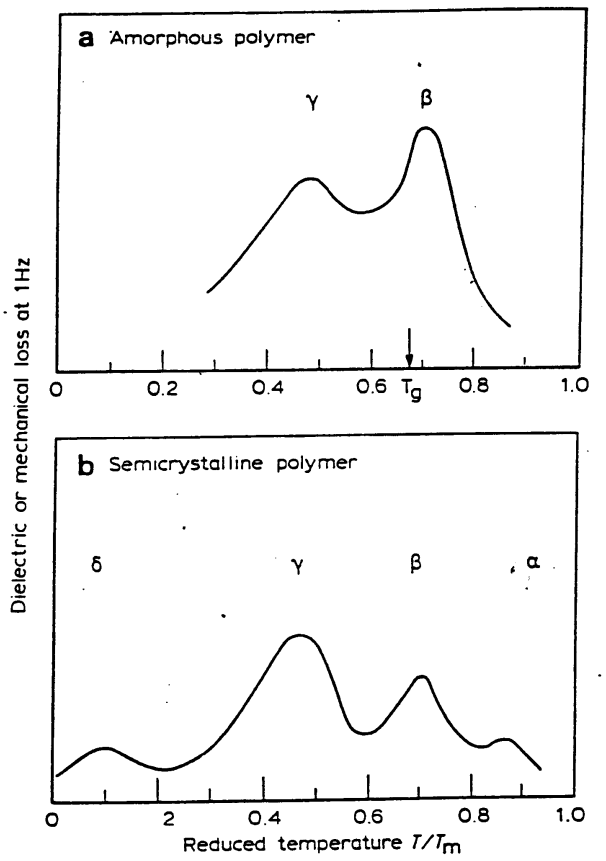

Figure 5.4: Schematic diagram of dielectric (or mechanical) loss in a) amorphous and b) semicrystalline polymers at 1 Hz; T_m is the crystal melting point in semicrystalline polymers[7]

The effects of temperature and frequency on loss mechanisms are directly related. Figure 5.5 illustrates the complex permittivity components of a polar amorphous polymer as a function of temperature in three frequency ranges. At low frequencies (DC to 1 kHz) the α peak, associated with main chain motion in this figure, exists just above the main chain T_g of the polymer. A β relaxation peak, due to local segment motion, distinctly exists above the local chain T_g' but below T_g. At very high temperatures, in the rubbery region, a λ peak occurs associated with ionic conduction. At intermediate frequencies (1 kHz to 100 kHz), the α and β peaks shift upward in temperature, with the separation between the peaks narrowing. The narrowing of the temperature gap between the α and β peaks is a result of the difference in activation energy behavior in the two loss mechanisms as the frequency increases.[6] The general upward shift of loss peaks along the temperature axis is a result of the need for greater molecular mobility for chains to rotate and relax under the influence of higher frequency excitation. This increased mobility is achieved at higher temperatures. Note that the ionic loss peak λ is greatly diminished at higher frequencies. At microwave frequencies the loss peaks have broadened and merged into a single relaxation peak beginning in the temperature range near T_g. This single peak is the result of increased free volume in the bulk allowing polar chain segment relaxation. Ionic loss contributions at microwave frequencies are negligible.

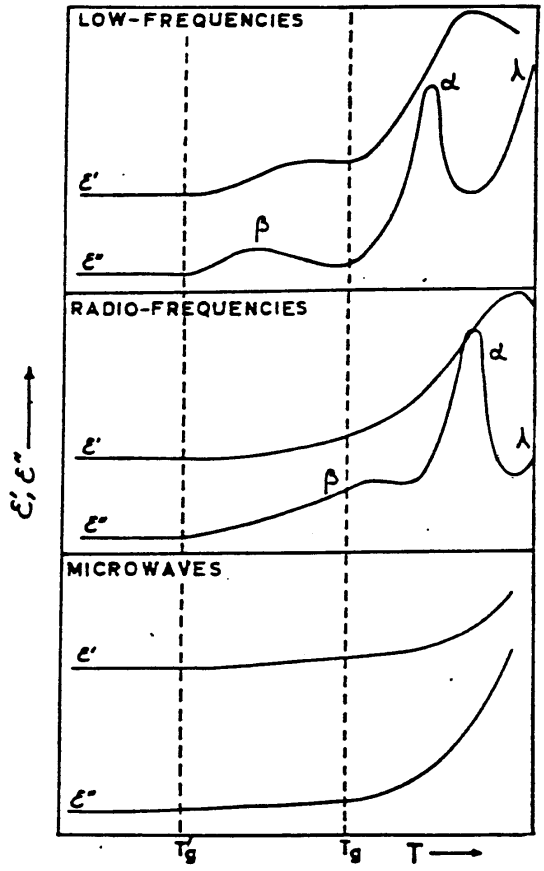

Figure 5.5: Schematic representations of model polymer dielectric properties as a function of temperature in three frequency ranges[9]

5.1.3 Physical Models of Permittivity and Loss

Molecular reorientation due to polarization of dipoles, also known as Debye dipole loss, is the primary electric field coupling mechanism in polymers.[1] A relationship exists between fundamental relaxation time constants for molecular rotation and relaxation (τ) and the period of oscillation, or equivalently the frequency ω, of the exciting electric field **E**. A quantitative approach to this phenomenon was developed by Debye in 1929, assuming spherical dipolar molecules in a viscous medium, described by

$$\text{Equation 5.10} \qquad \varepsilon^* = \varepsilon_\infty + \frac{(\varepsilon_S - \varepsilon_\infty)}{1 - j\omega\tau}$$

where ε_s and ε_∞ are the dielectric constants at very low frequency and very high frequency, respectively, ω is the circular frequency, and τ is the relaxation time constant.[10] When the electric field oscillates at a very low frequency relative to the relaxation time ($\omega \rightarrow 0$), $\varepsilon' \approx \varepsilon_s$ and $\varepsilon'' \approx 0$. This condition implies that the low frequency rotation of dipoles allows nearly total energy conservation, since the dipole can easily remain in-phase with **E**. At high frequencies ($\omega\tau \rightarrow \infty$), $\varepsilon' \approx \varepsilon_\infty$ and $\varepsilon'' \approx 0$. In this case, **E** oscillations are so rapid that

dipoles cannot begin to reorient, consequently a lower limit on the dielectric constant, ε_∞, is reached. This condition is analogous to diffraction in the optical region where the electric field merely changes velocity while traveling through a lossless medium.[1] There must exist an intermediate frequency range where there is maximum polarization-rotation phase-lag. This condition exists when $\omega\tau = 1$; at that frequency, the dielectric loss factor is a maximum ($\varepsilon'' = \varepsilon''_{max}$). Here the incident energy that was "stored" by a higher ε' at lower frequencies is now dissipated by loss mechanisms (i.e., a larger ε''). Figure 5.6, a typical plot of the components of ε^* over the frequency spectrum, illustrates the preceding arguments for ε_∞, ε_s, and the intermediate loss range.[1]

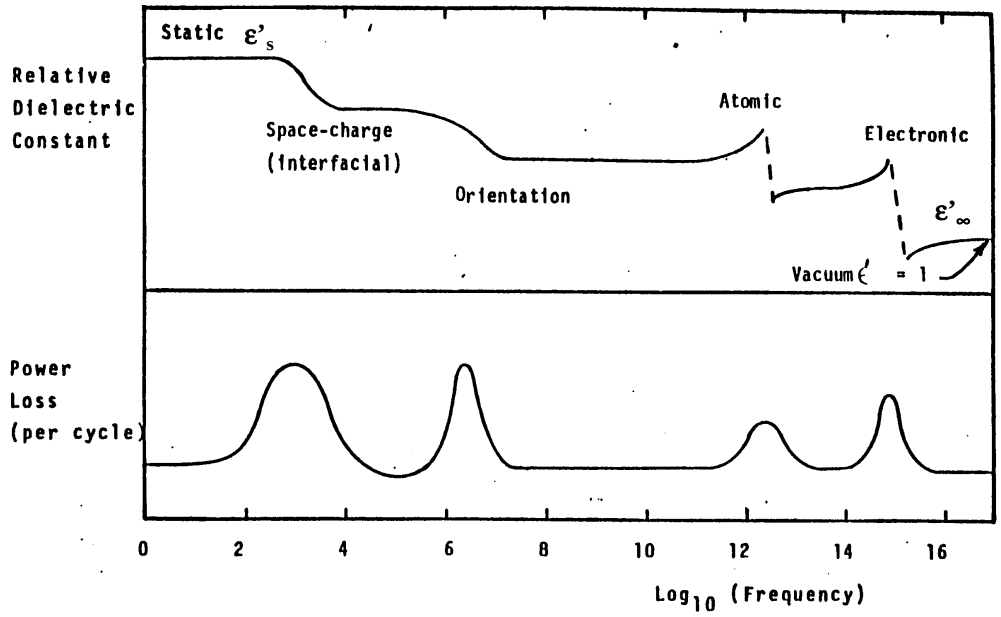

Figure 5.6: Approximate frequencies corresponding to polarization modes in polymers[11]

For the Debye model of Equation 5.10 to adequately model solid dielectric materials, it must account for the polarization effects due to adjacent molecules. To apply the Debye equations to solids, one must consider the activation energy necessary to rotate a polarized molecule against the potential gradients of the surrounding molecules in the material. A Debye time constant (τ_0) can be introduced into Equation 5.10 in place of τ

$$\text{Equation 5.11} \qquad \tau_0 = \frac{1}{\nu_0}\left(\frac{\varepsilon_s - 2}{\varepsilon_\infty + 2}\right)\exp\left(\frac{-U_a}{k_B T}\right)$$

where $(1/\nu_0)$ is the period of one oscillation in the "potential well" of the surrounding molecules, U_a is the activation energy, k_b is the Boltzmann constant, and T is absolute temperature. Note that the temperature dependence of this relaxation time constant is assumed to be statistically based and is of an Arrhenius form. Other relationships, including the WLF equation presented in Section 4.1.3.1, can be used to relate relaxation times with temperature for the T_g relaxation. The only material specific parameter in Debye's

simple model is the activation energy U_a. This single parameter limits the model to relatively narrow and symmetric relaxation spectra not consistent with actual polymer behavior.[6] Another well known relaxation model is that of the two-parameter Cole-Cole equation [10]

$$\text{Equation 5.12} \qquad \varepsilon^* = \varepsilon_\infty + \frac{(\varepsilon_s - \varepsilon_\infty)}{1 + (j\omega\tau)^\mu}$$

where τ is still the dipole relaxation time constant, and a new parameter μ is a measure of the interaction between the dipoles. This interaction is important in polymers where dipoles from the same chain, or from different chains, might strongly interact. This model yields better results for polymer relaxation spectra. A more advanced model that accounts for both the width and skewness of polymer relaxation spectra is the three-parameter Havriliak-Negami model; this model accurately describes T_g relaxation spectra.[12] The Havriliak-Negami model has the form

$$\text{Equation 5.13} \qquad \varepsilon^* = \varepsilon_\infty + \frac{(\varepsilon_s - \varepsilon_\infty)}{(1 + (j\omega\tau)^{1-\alpha'})^{\gamma'}}$$

where α' and γ' are the dispersion width and skewness parameters, respectively.

5.1.4 Electrical Modulus

Polymers and polymer matrix composites commonly exhibit very large apparent dielectric constants and loss when measured as a function of temperature at low frequencies (< 100 Hz). This phenomenon is attributed to several mechanisms including ionic conductivity caused by impurities, interfacial (Maxwell-Wagner-Sillars) polarization due to space charge buildup in heterogeneous materials, and inter-chain charge transfer through hydrogen bonds.[13,14,10] Domination of the dielectric relaxation response by these conductivity related processes can impede the analysis of dielectric spectra collected at low frequency. One proposed method of separating viscoelastic relaxations and conductivity effects has been proposed by Curtis[15] and implemented by Starkweather and others[14,16] in which the frequency dependent DC conductivity term ($\sigma/\omega\varepsilon_0$) in Equation 5.8 is subtracted from the overall dielectric loss as a function of frequency. An example of such a correction is shown in Figure 5.7 for Nylon 66. Drawbacks to this approach include: 1) either the DC conductivity of the material must be determined or a very low-frequency measurement of the dielectric loss be used to approximate the conductive term, and 2) the conductive mechanisms, such as interfacial effects, may not scale linearly with frequency.

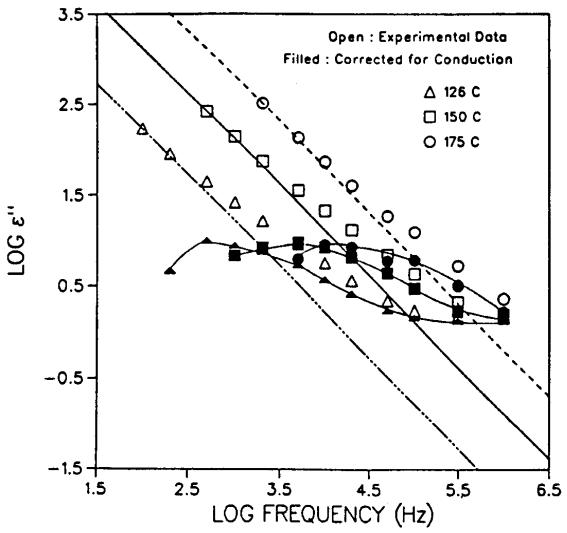

Figure 5.7: Dielectric loss in Nylon 66 in original form and corrected to remove conductivity effects[14]

Another approach is based on the electrical modulus representation of the constitutive relationship

Equation 5.14 $$\boldsymbol{D} = \varepsilon^* \boldsymbol{E}$$

In normal dielectric analysis the electric field, **E,** is assumed constant and the relaxation of the flux, **D,** is used to describe the permittivity of the system. In systems with mobile charges it is useful to consider **D** constant and describe the relaxation of **E** as

Equation 5.15 $$\boldsymbol{E} = M^* \boldsymbol{D}$$

The complex dielectric constant ε* is analogous to compliance in mechanical systems and can therefore be transformed in a similar manner as [13]

Equation 5.16 $$M^* = \frac{\boldsymbol{1}}{\varepsilon^*} = \frac{\varepsilon'}{\varepsilon'^2 + \varepsilon''^2} + j\frac{\varepsilon''}{\varepsilon'^2 + \varepsilon''^2} = M' + jM''$$

The advantage of using the modulus representation is that conductivity-dominated increases in the dielectric data are minimized by the appearance of ε'^2 and ε''^2 in the denominator, thereby revealing significant relaxation features of the spectrum. This allows for the study of relaxation processes at low frequencies, usually obscured by conductivity effects, without arbitrarily ignoring the contribution of any physical process. An example of the improvement in peak resolution by the electrical modulus representation is shown in Figure 5.8 where the T_g relaxation in Nylon 6 appears as only an inflection in the dielectric and tan δ loss curves, but is a clear peak in the M" data. Tsangaris and co-workers have compiled an excellent review of common dielectric analysis equations restated in terms of electrical modulus, including the Debye, Cole-Cole, Davidson-Cole, and Havriliak-Negami equations.[13] A useful point from this article states that relaxation times obtained from dielectric loss peaks do not correspond to those obtained from electrical modulus loss peaks, but must scale as

Equation 5.17 $$f_{M,\max} = \frac{M_\infty}{M_s} f_{\varepsilon,\max}$$

where $f_{M,max}$ and $f_{\varepsilon,max}$ are the frequencies corresponding to peak maxima in the modulus and dielectric representations, and M_∞ ($=1/\varepsilon_\infty$) and M_s ($=1/\varepsilon_s$) are the relaxed and unrelaxed electrical moduli, respectively. Of course relaxation times taken from peaks within spectra of the same representation (dielectric constant or electrical modulus) are directly comparable in viscoelastic analyses.

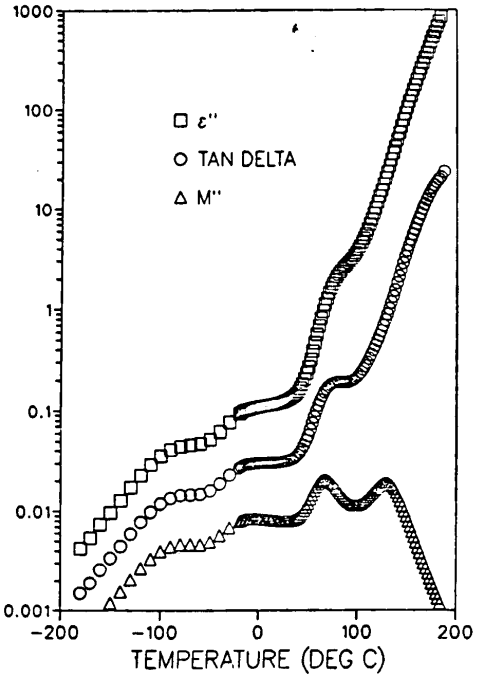

Figure 5.8: Relaxations in Nylon 6 at 1 kHz represented in terms of dielectric loss ε", tan δ, and electric modulus M" [13]

5.1.5 Dielectric Studies of Polymers and Composites

5.1.5.1 Polymer Blends and Plasticized Systems

The phase behavior of polymer blends has been studied by dielectric spectroscopy. Rellick and Runt used dielectric spectroscopy to characterize phase stability in blends of polyvinyl chloride (PVC) and ethylene-vinyl acetate (EVA) copolymers.[17] They found that beyond some critical EVA fraction of the blend, only a single α dielectric loss peak was observed, while phase separation occurred in blends with less EVA as manifested in α loss peak splitting. As the phase with the lower temperature T_g became more concentrated, its ionic loss contribution at trans-T_g temperatures increased, effectively masking the upper temperature peak. The authors employed an equivalent circuit model in which the DC conductivity term could be

factored out, yielding well-resolved split tan δ peaks. A Fox equation analysis was subsequently performed to determine the degree of mixing using the now resolved peaks. It was found that where previous Fox analyses based on T_g data taken from single tan δ peaks had failed, T_g data from the resolved peaks resulted in good agreement with Fox predictions based on pure component T_g data.

Pethrick and co-workers correlated dielectric relaxation spectra with peel strength results in an attempt to improve the method of material selection for heat seal adhesives.[18,19] The adhesives studied were mixtures of poly(methyl methacrylate) PMMA and poly (n-butyl methacrylate) PBMA with dicyclohexylphthalate (DCHP) , a meltable plasticizer that is a crystalline solid at room temperature. These mixtures would act as delayed action heat-sealing adhesives where the melting of the plasticizer would tackify the polymer. In order to establish the miscibility of these systems after heat activation, the Fox equation was employed using T_g data obtained from a mechanical penetration test. The T_g of the PBMA/DCHP mixture was found to agree well with the Fox prediction over the entire plasticizer concentration range. However, dielectric spectra showed peak splitting at higher plasticizer concentrations. It was determined that at high plasticizer fractions the observed relaxation was not that of plasticized polymer chains alone, but a combination of backbone chain motion and plasticizer relaxation characteristic of phase separation. This mixture could be tailored to provide dielectric relaxation times suitable for correlation with adhesive measurements. The relaxation times of these adhesives were computed as a function of temperature and compared with peel strength data for a polymer/glass bond. For data obtained at a fixed temperature, a linear relationship was found between dielectric loss measured at varied frequencies and peel data obtained at varied rates. This suggests that the rate dependent change of adhesion was directly related to viscoelastic relaxation in the adhesive.

5.1.5.2 Dielectric Relaxations and Cooperativity

The Debye model describes the relaxation of a single dipole in the frequency domain. If Equation 5.10 was transformed into the time domain, the single relaxation would have a time functional dependence of [20,21]

$$\text{Equation 5.18} \qquad f(t) \propto \exp\left(\frac{-t}{\tau}\right)$$

Just as the Cole-Cole and other frequency domain models were developed to explain more complex materials having broader or asymmetric relaxation spectra, a time domain approach is the stretched exponential form of the Kohlrausch, Watts and Williams (KWW) equation [20,21]

$$\text{Equation 5.19} \qquad \Phi(t) = \exp\left(-(t/\tau)^{1-n}\right)$$

where Φ is the relaxation, or time-decay, function and n is the coupling constant which is related to the breadth of the relaxation time distribution.[22] The values of n can vary from 0 to 1; if n=0 Equation 5.19 reduces to the behavior of a Debye-type relaxation. Because of their structure, polymer dipoles experience both intra- and intermolecular constraints on their motion, leading to broadened relaxation spectra and non-zero values of n.[23]

The influence of intermolecular interactions on the relaxation spectra of polymers was examined by Ngai and Roland.[24] These authors reasoned that the segmental motions of a given polymer chain at T_g were constrained by adjacent polymer chains, thereby retarding the relaxation of that individual chain from its unique unconstrained relaxation time. This constraining effect occurs throughout the polymer bulk, retarding the relaxation motions, and thereby broadening the distribution of relaxation times. In order for the ensemble of chains constrained through intermolecular coupling to relax through the glass transition, a large degree of cooperative motion is required.[25] Greater "cooperativity" in motion between the neighboring chain segments indicates a higher degree of correlation in their relaxation times.

The idea of cooperativity was linked to the KWW stretched exponential by Ngai and Plazek based the coupling model of Ngai[22]

$$\text{Equation 5.20} \qquad \tau^* = \left[(1-n)\,\omega_c^n \tau_0\right]^{\frac{1}{1-n}}$$

where τ_0 is the relaxation time due to intramolecular interactions, τ^* is the measured relaxation time, and ω_c^n is the coupling crossover frequency. The form of Equation 5.20 is very useful because it can be related to data obtained using simple viscoelastic time-temperature principles. If the ratio of relaxation time data, τ^*, measured at some arbitrary temperature T, is taken relative to that at a reference temperature T_R, then the result is simply the shift factor a_T. Using the definition in Equation 5.20 in the quotient, and realizing that ω_c^n is a constant which ratios to unity, then taking the logarithm yields

$$\text{Equation 5.21} \qquad (1-n)\log a_T = (1-n)\log\frac{\tau^*(T)}{\tau^*(T_R)} = \log\frac{\tau_0(T)}{\tau_0(T_R)}$$

If the reference temperature of Equation 5.21 is T_g, then the WLF equation can be used to describe the temperature relationship to the relaxation coupling constant n. Ngai and Plazek used a variation on the WLF equation having the form [24]

$$\text{Equation 5.22} \qquad (1-n)\log a_T = \frac{-C_1(T-T_g)/T_g}{C_2 + (T-T_g)/T_g}$$

to analyze a number of polymers, including an epoxy resin, as shown in Figure 5.9. This form of graph, where shift factor data is plotted as a function of normalized deviation from T_g, is referred to as a cooperativity plot. Excellent agreement was found between the shift factor data for these polymer systems and a general curve based on Equation 5.22. The authors reasoned that this fit indicated that the temperature dependencies of segmental motions were similar for all of the studied systems. Values of 5.49 and 0.141 were obtained for C_1 and C_2, respectively, from the ensemble plot of Figure 5.9.

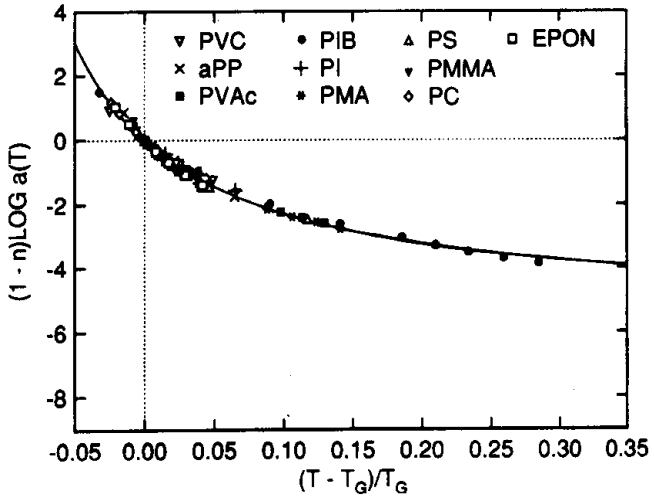

Figure 5.9: Cooperativity plot of a variety of polymers, scaled by the coupling constant, suggesting a common form of segmental motion in each system[22]

Activation energies of the glass transition can be extracted from the shift factor or cooperativity curve using an Arrhenius-type relationship based on the steepness index, S, which is the slope of the log a_T curve at T_g [26]

Equation 5.23 $$S = -T_g\left(\frac{d\log a_T}{dT}\right)_{T=Tg} = \left(\frac{d\log a_T}{d(T/T_g)}\right)_{T=Tg}$$

The activation energy is computed from

$$\log a_T \propto -\frac{E_{act}}{2.303RT}$$

Equation 5.24 $$E_{act} = 2.303RT_gS$$

Jensen used mechanical relaxation spectra obtained by DMA to successfully conduct a cooperativity analysis of latex epoxy neat resins and impregnated glass composites.[27,28] Cooperativity plots of relaxation data from samples of cured neat epoxy resin containing varied concentrations of surfactant are shown in Figure 5.10. The slopes of the curves in the normalized temperature region above T_g were suppressed (became less negative) as a function of added surfactant with an accompanying decrease in coupling constants, n. Jensen attributed these results to decreased intermolecular cooperative motion due to the presence of surfactant. The surfactant was reasoned to act as a plasticizer by increasing the free volume of the epoxy network, thereby diminishing the restrictions on motions by neighboring polymer chains. Another interpretation was that, since the T_g of the surfactant molecules was so far below that of the epoxy network, the surfactant molecular motion would be fully activated during the epoxy glass relaxation. Therefore the surfactant would not exert any intermolecular constraints on the epoxy chain motion during the epoxy glass transition. Only the cooperativity data above T_g were used in computing the coupling

constants because of poor agreement with the WLF curve (Equation 5.22) below T_g. This behavior was attributed to non-equilibrium behavior of the epoxy in the glassy state.

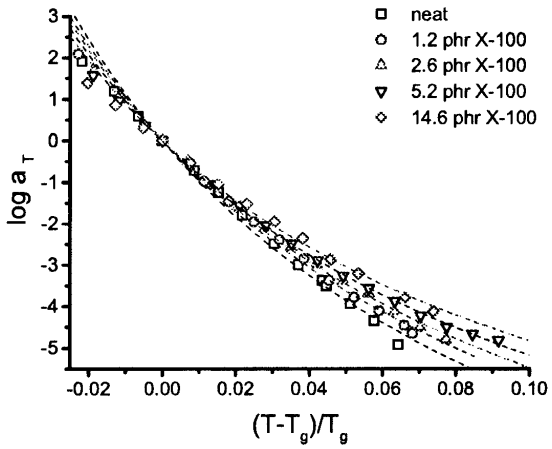

Figure 5.10: Cooperativity plot of unfilled epoxy resins as a function of surfactant concentration[27]

Jensen found similar cooperative relaxations in his DMA study of glass supported epoxy resins.[28] The coupling constants, n, for neat and glass-supported epoxy resins containing no surfactant were computed to be 0.63 and 0.71, respectively. The addition of glass reinforcement with a reactive sizing agent was thought to form chemical bonds with the epoxy network and thereby constrain segmental motions in the interphase. When epoxy resin containing 5.2 wt % surfactant was used as the matrix for the glass, a lower value of n, 0.60, was measured. Jensen suggested that if the surfactant segregated to the interphase, then the coupling between the fiber and matrix could be blocked. All of the previous results were obtained using an experimental epoxy emulsion. In parallel experiments, a commercial latex resin system was studied; values of n for bulk and glass-supported resins were found to be 0.57 and 0.59, respectively. This small increase was again attributed to surfactant migration to the glass/resin interface. It is important to note that the aforementioned commercial epoxy/surfactant matrix had been dried *prior* to impregnation of the glass. Another experiment was conducted using a waterborne epoxy resin to impregnate the glass. The coupling constant (n = 0.63) was found to be somewhat greater than that of the composite formed with the pre-evaporated resin. A cooperativity plot summarizing the commercial resin results is presented in Figure 5.11. Overall, the results indicated that surfactant reduced cooperative molecular motions in bulk resins with more significant effects in epoxy/glass composites due to disruptive interfacial surfactant interactions with the epoxy matrix.

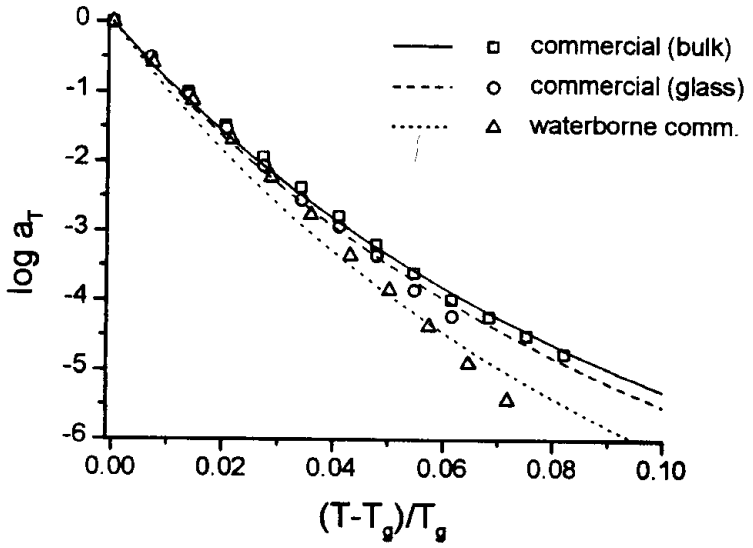

Figure 5.11: Cooperativity plots of unfilled and glass-supported commercial latex epoxy resin[28]

Ngai and Roland have applied cooperativity analysis to compatible blends of thermoplastics using dielectric spectroscopy.[25,29] A study of poly(vinyl methyl ether) (PVME) mixed with polystyrene (PS) yielded several insights into intermolecular coupling between segments of molecules having comparable coupling constants, but very different T_g values.[29] Their work examined the effects of different polymer compositions on molecular motions within segmental-scale "environments". It was found that the presence of higher T_g , and therefore slower relaxing, PS in PVME dominated environments increased the intermolecular coupling as reflected in a higher coupling constant. Furthermore, the relaxations measured by dielectric spectroscopy were predominantly those of the PVME because of its much greater dipole moment relative to PS. This allowed an almost exclusive examination of the PVME environments that could not be duplicated by mechanical techniques. The association between the coupling parameter in PVME environments and the activation energies associated with their relaxations was verified; greater cooperativity among the segmental motions correlated with shift factors having an increased dependence on temperature as reflected in the "steepness" of the curves in a cooperativity plot.

Ngai and Roland reported a similar study performed by their group on blends of tetramethyl-Bisphenol A polycarbonate (TMPC) and PS.[25] Again dielectric spectroscopy was used with TMPC as the primary phase of investigation due to its larger dipole moment. In this case there were very large differences in both coupling constants and T_g between the polymers, with PS having smaller values for both. The authors expected to find that local (segmental) environments of TMPC, which contain some fraction of PS, would exhibit lower intermolecular coupling and therefore a lower correlation constant. Also, since PS would be well above its T_g when the TMPC chains started to relax, the constraints imposed by the PS chains on the TMPC segment motion would be minimal. Based on the coupling concept of Ngai (Equation 5.21), a stronger cooperative motion in the TMPC would be expected to correlate with a greater dependence of the

relaxation on temperature. These expectations were borne out as shown in the cooperativity plot of Figure 5.12. The slope of the pure TMPC curve shows the steepest dependence on temperature, with a gradual decrease in steepness with increased PS concentration. The authors made the important point that the relaxations measured for a blend represent a sum over a statistical distribution of coupling constants corresponding to a spectrum of local environments. Therefore a smaller n in this blend corresponded with local environments of TMPC enriched with PS instead of an overall average of the blend.

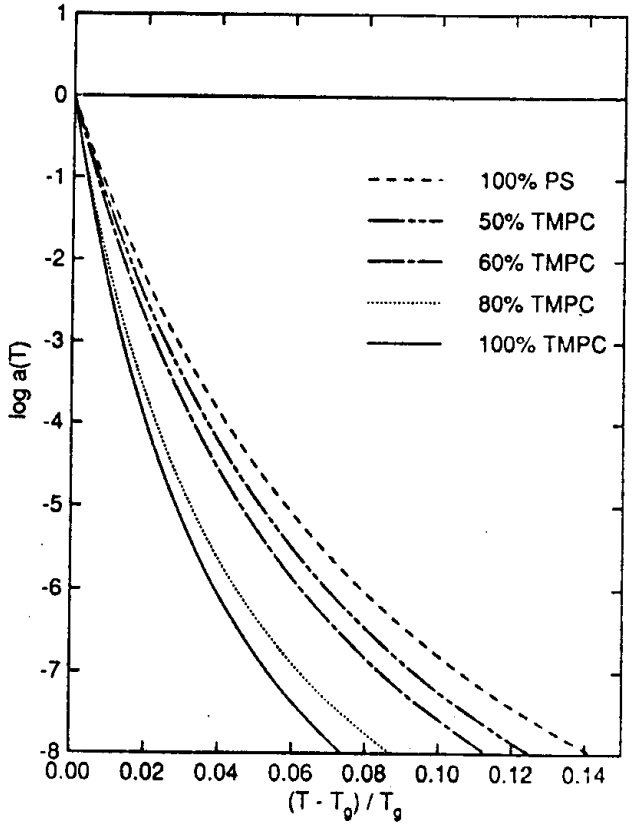

Figure 5.12: Cooperativity plot of a TMPC/PS blend as a function of PS concentration[25]

5.1.6 Electrical Performance of Interlayer Dielectric Laminates

Conductor traces in multilayer PCB constructions can be considered as waveguides surrounded by a dielectric medium. The characteristics of the electromagnetic waves propagating along these conductors are defined by the dielectric properties of the surrounding interlayer laminates. Two critical performance parameters are the wave velocity, which is critical in determining the frequency limitations of the circuit, and the attenuation coefficient that governs the transmitted signal integrity. The wave velocity v_p is dependent on the dielectric constant as[30]

$$\text{Equation 5.25} \qquad v_p \propto \frac{1}{\sqrt{\varepsilon'}}$$

and the attenuation coefficient, α_ε, due to dielectric loss in the medium is given by

Equation 5.26 $$\alpha_\varepsilon \propto \tan\delta \sqrt{\varepsilon'}$$

The laminate materials fabricated for this study are very similar in composition to commercial PCB substrates designated FR-4, with the main difference being that the DGEBA epoxy resin is not brominated for flammability suppression. Literature values for FR-4 dielectric properties will be used as a performance benchmark for comparing the solventborne epoxy and waterborne latex resin impregnated laminates. ASTM standard D 1867 quotes maximum dielectric properties at 1 MHz for FR-4 laminates of all thicknesses to be ε_{max}' = 5.4 and ε_{max}" = 0.189.[31] Average values for FR-4 at 100 kHz are reported as ε' = 4.65 and ε" = 0.0837.[32]

5.2 Results and Discussion

5.2.1 Dielectric Properties and Modulus Representations

The dielectric properties of neat resin and laminate samples were measured in a step-isothermal mode at the frequencies 0.03, 0.1, 1, 10, 100, 1k, 10k, and 100 kHz. A maximum measurement temperature of 250°C was necessary to obtain as much spectral relaxation data as possible without degrading the epoxy samples. Since such high temperatures were reached during each measurement, no systematic evaluation of postcure behavior was feasible. Samples were measured in the as-made condition, then re-measured in-situ. The second measurement was considered to be of fully cured material; all data reported here are correspond to these second measurements.

Data taken at 100 kHz can be considered a reasonable estimate of the MHz range properties that are important in digital circuit constructions. Dielectric data for neat resin materials, measured at 100 kHz, are shown in Figure 5.13 A and B. The values for ε' (Figure 5.13 A) fall in a range from 2.75 to 3.5 at room temperature, with the solventborne and 5 wt% surfactant latex resins having the higher dielectric constants. These results generally agree with literature values of ε' = 3.0 – 3.6 measured in the 100 kHz to 1 MHz frequency range.[33,34] Room temperature dielectric loss values, ε", shown in Figure 5.13 B for all of the neat resins, are less than 0.1; Mumby and Schwarzkopf quote a 1 MHz value of ε" = 0.115 for neat samples of standard FR-4 laminating resin.[35] Note that the dielectric loss increases dramatically in the 50°C to 100°C range with the resins containing greater surfactant concentrations diverging at lower temperatures. This increase in loss is attributable to a combination of greater dipole relaxation ($\varepsilon"_{dp}$) and mobility of conductive species (σ) associated with the onset of the glass transition. The depression of T_g by plasticization is reflected in the lower temperature divergence of the 15 wt % surfactant epoxy material.

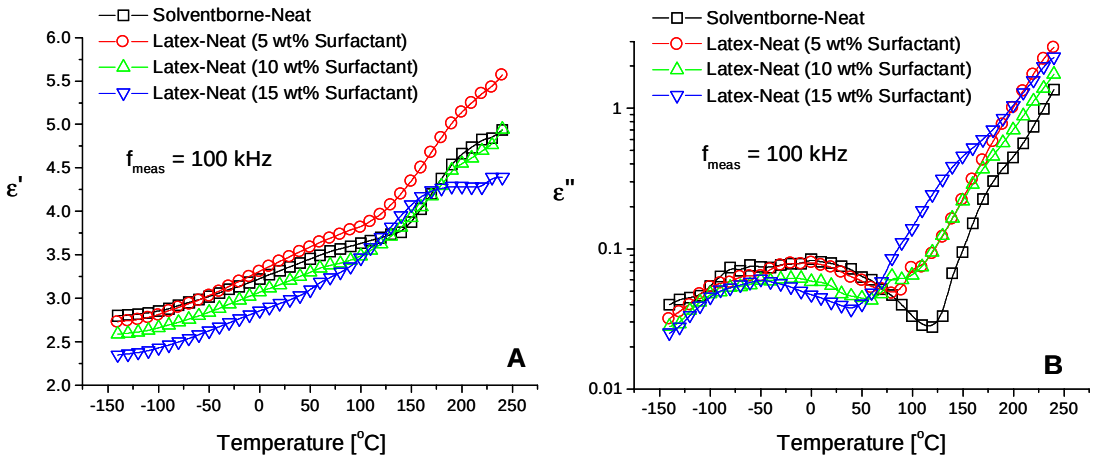

Figure 5.13: Dielectric constant and loss factors of neat epoxy resins at 100 kHz

Laminate dielectric properties, measured as a function of temperature, are shown in Figure 5.14 A and B. The room temperature measurements of ε' for the experimental laminates are somewhat lower than the 4.65 value cited in Section 5.1.6, while the ε" results agree well with the cited loss value of 0.084. Note that the depression of T_g is again observed in the laminates fabricated with high-surfactant loadings. It must be reiterated that the resins used in this study were not brominated, and that the literature values for laminate materials vary significantly based on the mass fraction of glass in the composite. Nevertheless, the dielectric properties measured for the model laminates are generally within specification for actual interlayer dielectrics, even in the case of resins containing added surfactant.

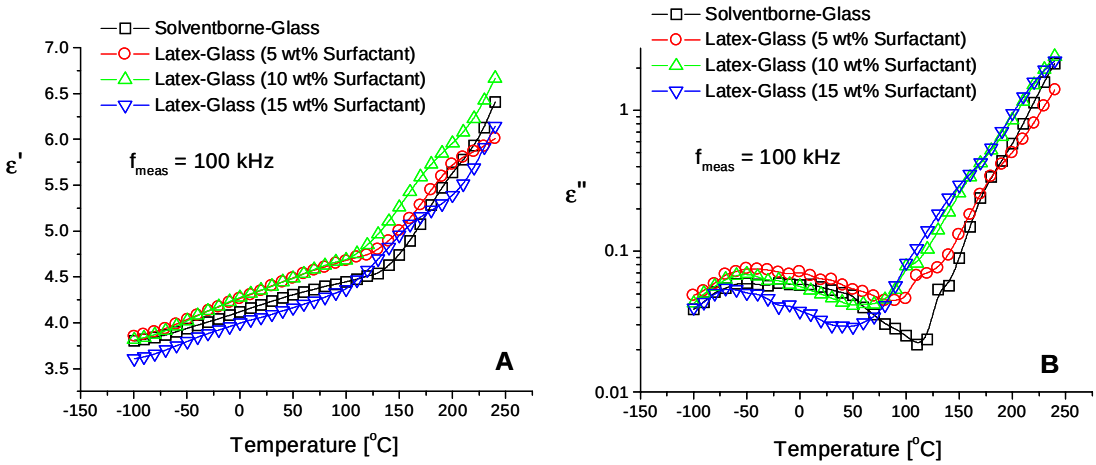

Figure 5.14: Dielectric constant and loss factors of glass/epoxy laminates at 100 kHz

The glass transition peaks in Figure 5.13 and Figure 5.14 are masked by conductivity effects, appearing only as inflection points on monotonically increasing ε" curves. A more dramatic example of this effect is seen at lower frequencies where DC conductivity has greater influence. Figure 5.15 A and B are plots of ε' and ε" for laminate materials measured at 1 Hz. Note that, over the same temperature range seen in Figure 5.13 and Figure 5.14, the dielectric properties in Figure 5.15 increase by several orders of magnitude. No reasonable values of T_g could be determined from the slight inflection points along the exponentially increasing loss curves. However, if the same data is recast in terms of the electrical modulus, as presented in Figure 5.16 A and B, distinct peaks are observed in the M" data, while the M' curve is bound within a reasonable range. For this reason all of the dielectric data measured in this study were converted to the electrical modulus form for further viscoelastic analysis.

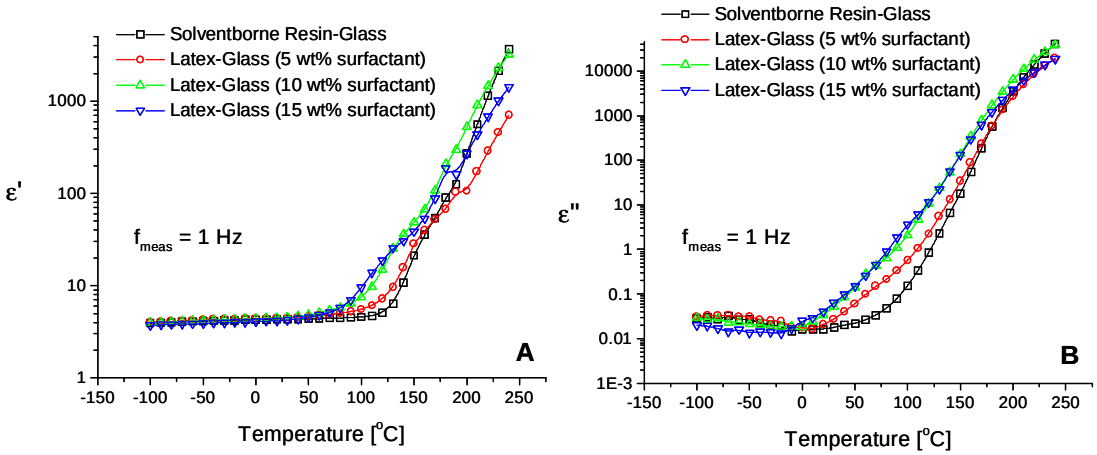

Figure 5.15: Dielectric properties of glass/epoxy laminate measured at 1 Hz showing high temperature conductivity masking of the T_g relaxation

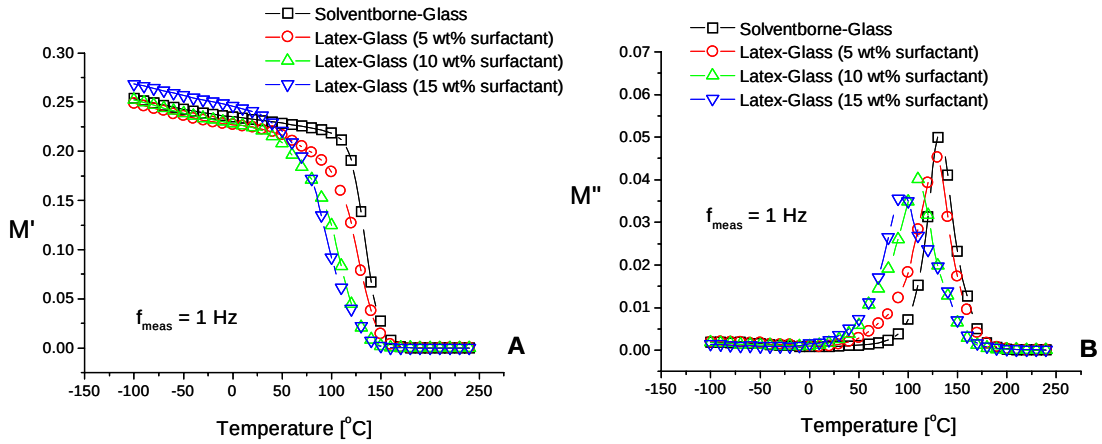

Figure 5.16: Electrical modulus representation of the same glass/epoxy laminate shown in Figure 5.15; T_g relaxation peaks are well resolved in the M" plot (B)

5.2.2 Cooperativity Analysis

Typical M" results, measured at the frequencies listed previously, are presented in Figure 5.17 as a function of temperature. These relaxation peaks were fit with Lorentzian curves, as described for DMA relaxation data in Section 4.2.3, and the resulting calculated peak temperatures were recorded. Each peak temperature/frequency data point represents a relaxation time τ (T), since τ = (1/frequency). The ratio of these τ (T) values to a relaxation time at a reference temperature τ (T_R) will give a family of shift factors, a_T, as defined in Equation 5.21. The peak temperature at 1 Hz was selected as the reference temperature, and designated as the T_g for that material system. A comparison of log a_T versus the normalized temperature deviation from T_g yields a cooperativity plot as shown in Figure 5.18. The data in Figure 5.18 were fit, using the nonlinear curve-fitting feature of the Origin™ software, to an equation having a form similar to Equation 5.22:

$$y = \frac{-A1 * C1 * x}{C2 + x}$$

Equation 5.27

where

$$y = \log a_T, \; x = \frac{T - T_g}{T_g}, \; A1 = \frac{1}{1-n}$$

and C1 and C2 are the WLF-like constants found by Ngai and Plazek [22] to be 5.49 and 0.141, respectively. Since the calculated coupling constant, n, values are to be used only for relative comparisons, the arbitrary selection of these C1 and C2 values will have no effect on the results. Activation energies of the glass transition were computed using Equation 5.23 and Equation 5.24.

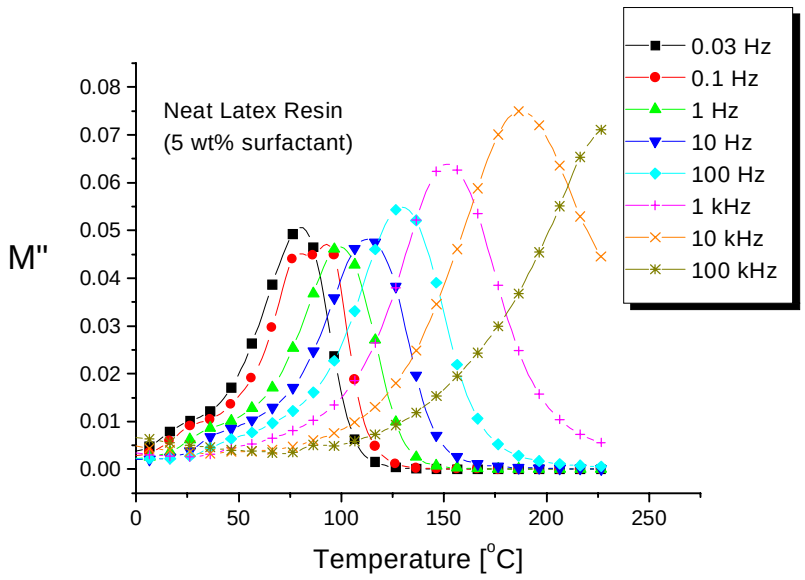

Figure 5.17: Electrical loss modulus T_g relaxations at various frequencies for cured 5 wt % surfactant neat latex epoxy resin

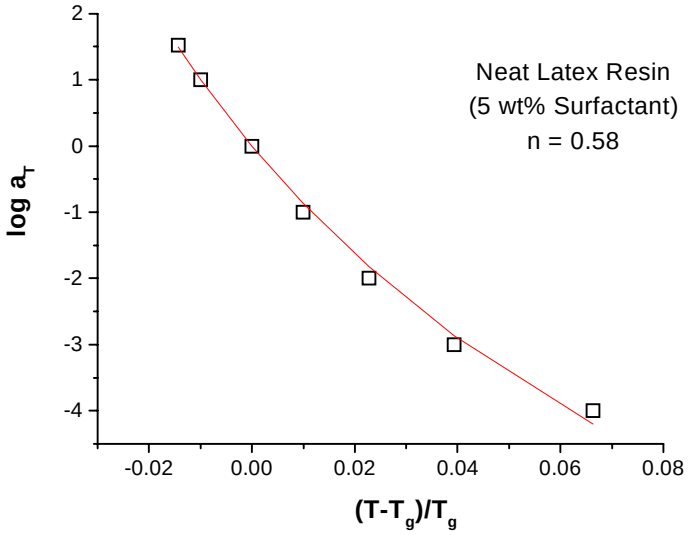

Figure 5.18: Cooperativity plot for a 5 wt % surfactant neat latex epoxy resin with a curve fit corresponding to Equation 5.27

Cooperativity plots for solventborne and latex neat epoxy resins are presented in Figure 5.19. Glass transition temperatures, activation energies and coupling constant data are given in Table 5.1. The

tabulated statistics represent averages of three samples. The standard deviation values for the coupling constants do not account for the error of curve fitting by Equation 5.27; the maximum observed χ^2 parameter of the curve fits was 0.075. Error bars in Table 5.1 represent the standard deviations in $(T-T_g)/T_g$ arising from the uncertainty in peak temperature measurement.

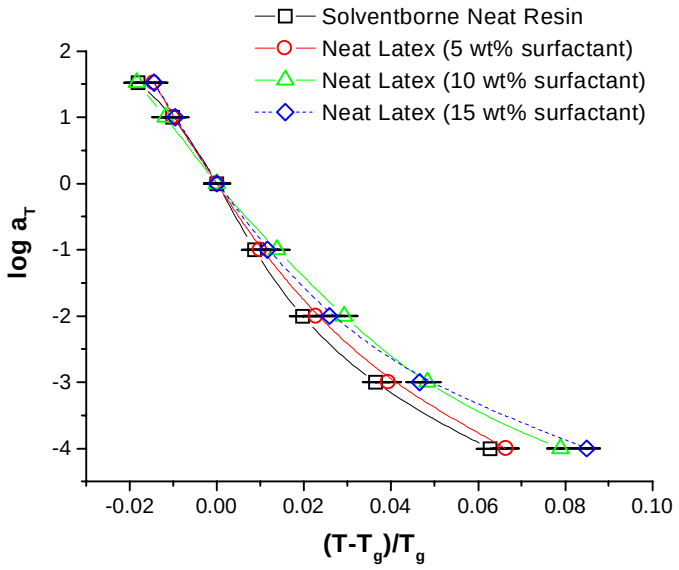

Figure 5.19: Cooperativity plots for neat epoxy resins containing varied surfactant concentrations

Neat Resin Type	T_g [K] @ 1 Hz (σ [K])	E_{act} [kJ/mol] (σ [kJ /mol])	n	σ_{max} (Estimated)
Solventborne Resin	403.3 (2.9)	741 (42)	0.59	0.003
Latex Resin (5 wt % Surfactant)	386.0 (1.4)	735 (88)	0.58	0.009
Latex Resin (10 wt % Surfactant)	367.1 (3.4)	550 (24)	0.51	0.005
Latex Resin (15 wt % Surfactant)	361.4 (1.1)	636 (29)	0.52	0.009

Table 5.1: Relaxation parameters for neat epoxy resins

Neat resin T_g values decreased with added surfactant due to plasticization of the network. The activation energies and coupling constants for the solventborne and 5 wt % surfactant resins are similar in magnitude, while those for the resins containing additional surfactant have significantly lower values values. Smaller activation energies and n values for the 10 and 15 wt % surfactant resins are consistent with plasticizer disrupting the segmental cooperative motions in the network as observed by Jensen.[27] The similarity between the n and E_{act} values for the solventborne and 5 wt % surfactant neat resins is surprising. Although the glass transition temperature of the 5 wt % surfactant resin was depressed, the local segmental

cooperative motions were not "screened" by the surfactant molecules. This result suggests two possibilities: a threshold concentration of surfactant below which segmental cooperative motion is only slightly disrupted, or that the dielectric technique employed in this study is preferentially probing the relaxations of local segmental environments depleted of surfactant. The latter of these explanations would indicate inhomogeneity of surfactant distribution on the scale of local segmental environments, despite overall miscibility with the epoxy network. No definitive conclusions as to the exact mechanism can be drawn here. However, if the work of Ngai and Roland on TMPC/PS blends is revisited in Figure 5.12, it is clear that the slopes of the 100% and 80% TMPC curves are similarly steep, but that an interval exists between these curves and curves for blends with greater PS concentration.[25] The n values corresponding to these cooperativity curves were not tabulated in their report, but a process similar to the one in this study may be responsible.

Cooperativity plots for laminate materials fabricated with solventborne and latex resins are presented in Figure 5.20. Glass transition, activation energy and coupling constant data for these laminates are listed in Table 5.2. Glass transitions are again depressed with increased surfactant concentration although the T_g values for the solventborne and 5 wt % surfactant resin are similar; these results will be discussed further in terms of a Fox equation analysis. Activation energy and coupling constant values for the solventborne-matrix laminates are very similar to those measured for the neat solventborne resin, suggesting that the dielectric measurements are probing the relaxations of local matrix epoxy segmental environments unperturbed by the influence of the fiber/matrix interphase. These results are fundamentally different from those obtained by mechanical testing where the motions of the fibers relative to the matrix influence the relaxation spectrum. A significant decrease was measured in the activation energy and coupling constant of the 5 wt % surfactant resin/glass laminate relative to the same resin in a neat form. It is believed that these findings are attributable to increased plasticizer interaction with the relaxing chain segments in local environments enriched with surfactant. Since this local surfactant enrichment corresponds to the addition of a glass reinforcement phase, it follows that relaxations of local environments near the glass surface are being preferentially probed by the dielectric measurements. These results reinforce the concept of a plasticized fiber interphase region hypothesized in Chapter 4. Activation energies and coupling constants measured for the 10 and 15 wt % surfactant resin/glass laminates are very similar, but these values are smaller than those of the 5 wt % surfactant laminate in keeping with the neat resin results.

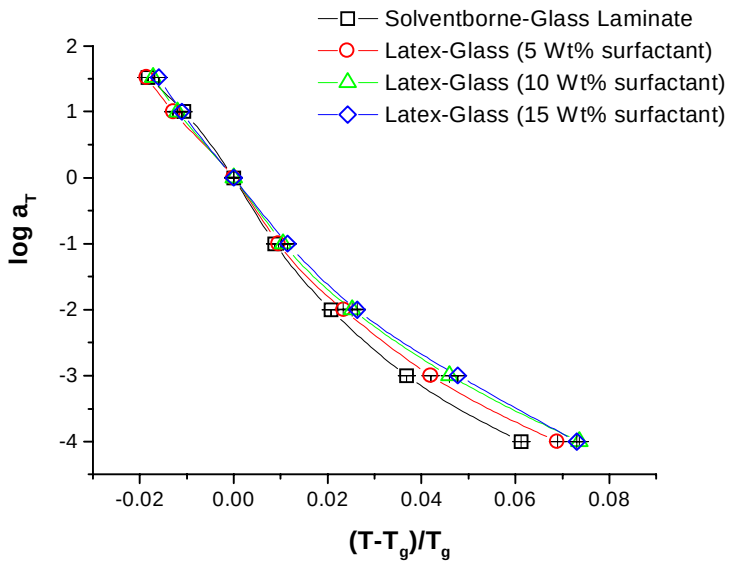

Figure 5.20: Cooperativity plots for glass/epoxy laminates containing varied surfactant concentrations

Laminate Material Resin Type	T_g [K]@ 1 Hz (σ [K])	E_{act} [kJ/mol] (σ [kJ /mol])	n	σ_{max} (Estimated)
Solventborne Resin	404.8 (1.5)	726 (50)	0.59	0.004
Latex Resin (5 wt % Surfactant)	401.5 (1.2)	661 (69)	0.55	0.009
Latex Resin (10 wt % Surfactant)	382.2 (1.7)	626 (25)	0.54	0.006
Latex Resin (15 wt % Surfactant)	366.2 (1.3)	604 (12)	0.54	0.006

Table 5.2: Relaxation parameters for glass/epoxy laminates

5.2.3 Fox Equation Analysis

Jensen measured the T_g of Triton X-100 surfactant by DSC analysis to be –59°C.[28] His finding was confirmed in this work by DEA, as shown in Figure 5.21, where the peak of the M" plot was -56.7°C. Liquid Triton X-100 was spread on the interdigitated electrodes of the planar DEA sensor and allowed to level for several minutes (in a dry nitrogen atmosphere to minimize water adsorption) prior to measurement. This value of T_g was used in all further Fox equation analyses.

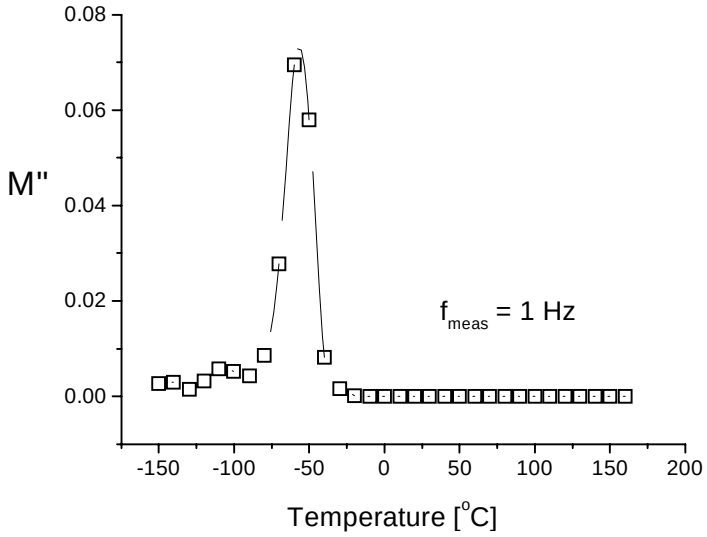

Figure 5.21: Electrical loss modulus T_g peak measured for Triton X-100 at 1 Hz

The glass transition temperature data listed in Table 5.1, measured by DEA at 1 Hz, is plotted in Figure 5.22 along with the predictions of the Fox equation (Equation 4.18) where the T_g of the solventborne resin represents the pure epoxy phase. The Fox equation prediction agrees well with the experimental T_g values signifying good overall miscibility of the epoxy network with the surfactant molecules; this finding verifies the results obtained by DMA in Section 4.2.3.1.1.

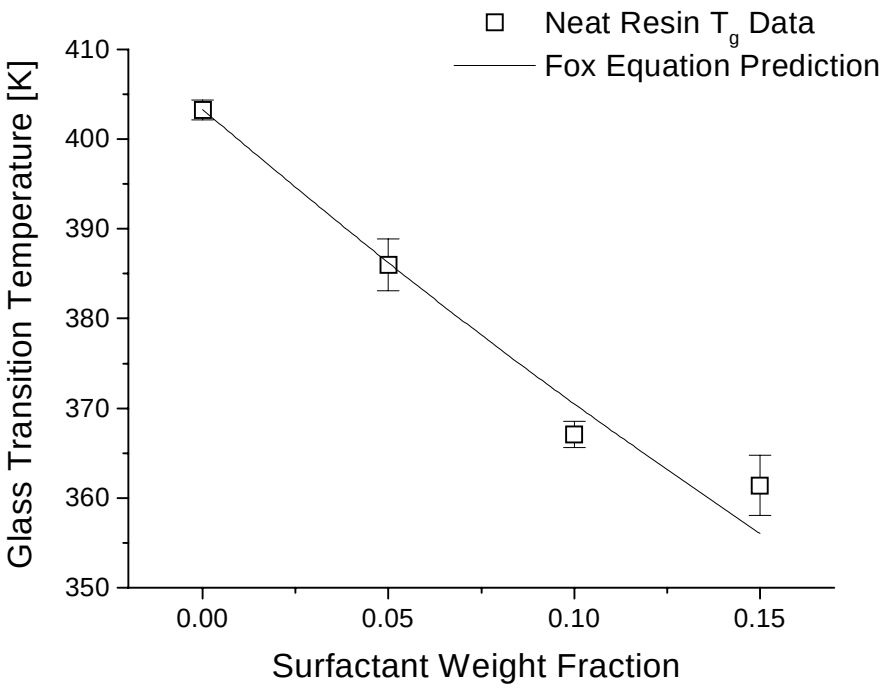

Figure 5.22: T_g data and Fox equation predictions for neat epoxy resins containing surfactant

Laminate T_g data from Table 5.2 and Fox equation predictions are presented in Figure 5.23. Note that the Fox equation results based on the solventborne resin under-predict the glass transition temperatures of the latex impregnated laminates in a manner similar to the DMA data described in Section 4.2.3.1.2. It was hypothesized in Chapter 4 that the T_g of unplasticized cured latex resin in a glass supported system was higher than the T_g of a glass filled solventborne system due to differences in DICY curing agent distribution. Furthermore, a decrease in T_g of 18.5°C was observed going from the as-made to the fully postcured states of 5 wt % surfactant resin impregnated laminate, attributable to surfactant diffusion and more complete plasticization. The 18.5°C temperature difference can be applied to the postcured T_g for the 5 wt % surfactant laminate as determined by DEA, thereby effectively modeling the unplasticized state of the as-made matrix resin. This shifted T_g value served as the unplasticized epoxy resin basis for the Fox prediction shown in the dashed upper curve of Figure 5.23; excellent agreement is shown between this prediction and the postcured T_g data determined by DEA. These results are further support of the hypotheses of Section 4.2.3.1.2 concerning surfactant segregation to the fiber interface in latex impregnated laminates.

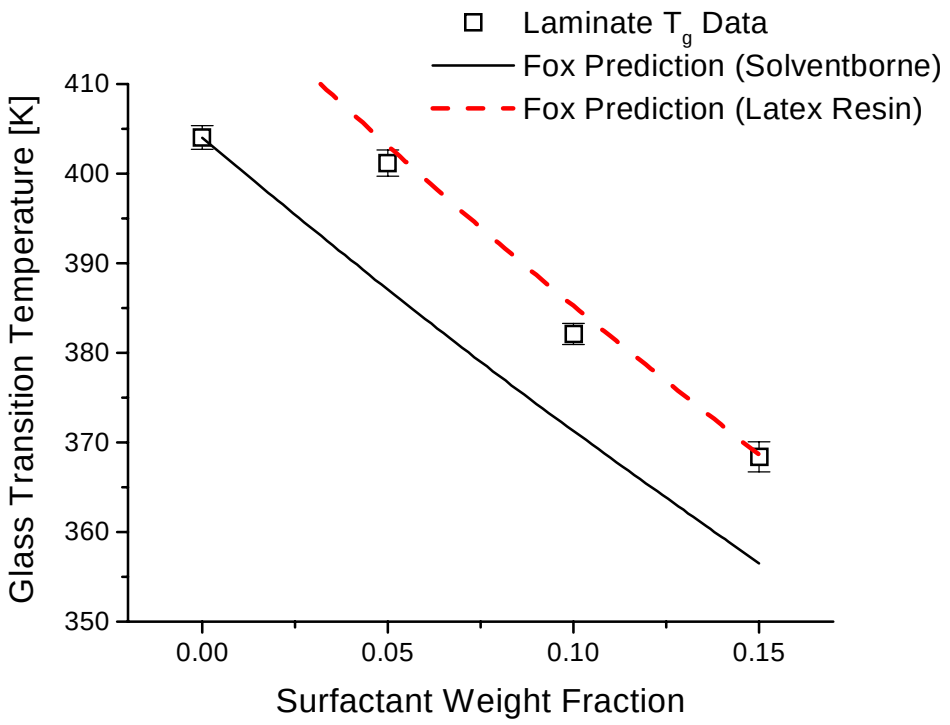

Figure 5.23: T_g data and Fox equation predictions for glass/epoxy laminates containing surfactant

5.3 Summary

The dielectric properties of neat epoxy films and epoxy matrix/glass laminates have been analyzed both in the context of performance as an interlayer dielectric and to gain a better understanding some of the fundamental processes impacted by the presence of residual surfactant. Laminate dielectric constant and loss factor data, measured at 100 kHz, met or exceeded performance criteria set forth in the literature, even when loaded with an extra 10 wt % surfactant. The presence of excess surfactant, beyond the 5 wt % found in the as-received commercial resin, was only deleterious in that it significantly depressed the T_g of the laminate, thereby lowering its maximum use temperature. The latex epoxy used in this study was not an electrical grade resin. This was evident in the large DC conductivity effects observed at lower frequencies and temperatures in excess of T_g. An electrical modulus representation of the dielectric data that minimized these conductivity effects was successfully employed in resolving relaxation peaks for further analysis.

The technique of applying a cooperativity analysis revealed information about the segmental relaxations at T_g in the solventborne and latex resins. The coupling constant for neat 5 wt % surfactant epoxy was calculated to be larger than that of the same resin in the form of glass reinforced matrix. These results suggest the segregation of surfactant to the glass/epoxy interphase, further supporting the hypotheses

formed in previous chapters. Analysis of neat resin T_g data, measured by DEA, resulted in good agreement with Fox equation predictions. This verifies full miscibility of the neat epoxy network by the surfactant molecules. However, the latex resin epoxy/glass laminate T_g data was under-predicted by the Fox equation based on the T_g of solventborne resin matrix material. When a higher T_g representing a cured, unplasticized 5 wt % surfactant latex resin/glass laminate was used in the Fox equation, the predictions agreed well with T_g data. This approach was similar to that of Section 4.2.3.1.2 for DMA results. Overall, these results support the hypotheses developed in Chapter 4 that complex DICY and surfactant effects occur at the glass/epoxy interphase.

5.4 References

[1] A. C. Metaxas and R. J. Meredith, Industrial Microwave Heating, Peter Peregrinus Ltd., London, 1983.

[2] C. A. Balanis, Advanced Engineering Electromagnetics, John Wiley and Sons, New York, 1989.

[3] A. R. von Hippel, Dielectrics and Waves, John Wiley and Sons, New York, 1954.

[4] W. D. Kingery, H. K. Bowen, and D. R. Uhlmann, Introduction to Ceramics, John Wiley and Sons, New York, 1976.

[5] M. Chen, Ph. D. Dissertation, VPI & SU, 1989.

[6] E. Jabbari, M. S. Thesis, VPI & SU, 1989.

[7] A. J. Bur, Polymer, Vol. 26, 1985, p. 963-977.

[8] M. B. M. Mangion, M. Wang, and G. P. Johari, Journal of polymer Science: Part B: Polymer Physics, Vol. 30, 1992, p. 445-453.

[9] V. Frosini, E. Butta, and M. Calamia, Journal of Applied Polymer Science, Vol. 11, 1967, p. 527-551.

[10] N. G. McCrum, B. E. Read, and G. Williams, Anelastic and Dielectric Effects in Polymeric Solids, Dover Publications, Inc., New York, 1967.

[11] C. R. Vail, Electro-Technology Science and Engineering Series, No. 38. 1962, p. 82-98.

[12] S. Havriliak and S Negami, Journal of Polymer Science: Part C, Vol. 14, 1966, p. 99-117.

[13] G. M Tsangaris, G. C Psarras, and N. Kouloumbi, Journal of Materials Science, Vol. 33, 1998, p. 2027-2037.

[14] H. W. Starkweather and P. Avakian, Journal of Polymer Science: Part B: Polymer Physics, Vol. 30, 1992, p. 637-641.

[15] A. J. Curtis, Journal of Research of the National Bureau of Standards, Vol. 65A, 1961, p. 185.

[16] M. Connolly, F. Karasz, and M. Trimmer, Macromolecules, Vol. 28, 1995, p. 1872-1881.

[17] G. S. Rellick and J. Runt, Journal of Polymer Science: Polymer Physics Edition, Vol. 24, 1986, p. 279-302.

[18] R. J. Elwell, D. Hayward, and R. A. Pethrick, Plastics, Rubber and Composites Processing and Applications, Vol. 17, 1992, p. 275-287.

[19] R. J. Elwell, D. Hayward, and R. A. Pethrick, International Journal of Adhesion and Adhesives, Vol. 13, 1993, p. 9-14.

[20] A. K. Jonscher, Universal Relaxation Law, Chelsea Dielectrics Press, London, 1996.

[21] T. Park, Ph D Dissertation, VPI&SU, 1994.

[22] D. J. Plazek and K. L. Ngai, Macromolecules, Vol. 24, 1991, p. 1222-1224.

[23] B. Fitz, S. Andjelic, and J. Mijovic, Macromolecules, Vol. 30, 1997, p. 5227-5238.

[24] C. M. Roland and K. L. Ngai, Macromolecules, Vol. 24, 1991, p. 5315-5319.

[25] K. L. Ngai, C. M. Roland, J. M. O'Reilly, and J. S. Sedita, Macromolecules, Vol. 25, 1992, p. 3904-3909

[26] J. J. Aklonis and W. J. MacKnight, Introduction to Polymer Viscoelasticity, Second Edition, John Wiley and Sons, New York, 1983.

[27] R. E. Jensen, Ph.D Dissertation, VPI & SU, 1999.

[28] R. E. Jensen, E. O'Brien. J. Wang, J. Bryant, T. C. Ward, and D. A. Lewis, Journal of Polymer Science: Part B: Polymer Physics, Vol. 36, 1998, p. 2781-2792.

[29] C. M. Roland and K. L. Ngai, Macromolecules, Vol. 25, 1992, p. 363-367.

[30] D. M. Pozar, Microwave Engineering, Addison-Wesley Publishing Company, Reading, Mass., 1990.

[31] ATSM Standard D 1867-94, Standard Specification for Copper-Clad Thermosetting Laminates for Printed Wiring"

[32] C. G. Henningsen and S. A. Gause, "Base Materials", in Printed Circuits Handbook, 4th Edition, Ed. C. F. Coombs, McGraw-Hill, New York, 1996.

[33] L. D. Olson, "Resins and Reinforcement", in ASM Electronic Materials Handbook: Vol. 1. Packaging, ASM International, Materials Park, OH, 1989.

[34] H. Lee and K. Neville, Handbook of Epoxy Resins, McGraw-Hill, New York, 1982.

[35] S. J. Mumby and D. A. Schwarzkopf, "Dielectric Properties and High-Speed Electrical Performance Issues", in ASM Electronic Materials Handbook: Vol. 1. Packaging, ASM International, Materials Park, OH, 1989.